Supplement of

Effects of photosymbiosis and related processes on planktic foraminifera-bound nitrogen isotopes in South Atlantic sediments

Alexandra Auderset et al.

Correspondence to: Alexandra Auderset (a.auderset@soton.ac.uk)

Size-specific $\delta^{18}O$ relationship. It has been proposed that due to persistently shallower depth habitats throughout ontogeny of symbiont-bearing foraminifera, their size-specific $\delta^{18}O$ relationship should be minimal in comparison to symbiont-barren foraminifera species with a larger potential range of depth habitats (Rebotim et al., 2017). The five species analysed in this study generally follow the data compilation-averaged species-specific predictions of size-specific $\delta^{18}O$ trends for dinoflagellate-bearing, chrysophyte-bearing, and symbiont-barren species in (Ezard et al., 2015) (Fig. S2) with *G. truncatulinoides* showing the biggest variation in $\delta^{18}O$ across the size fractions and *G. ruber ruber* showing the least variation. However, both *G. ruber ruber* and *G. siphonifera* seem to diverge from the general pattern in the size-specific stable isotope compilation (Fig. S2 b,c,e) by up to 0.5‰. A possible explanation for this could be the cooler waters at our site in comparison to the more tropical sites used in the compilation.

Influence of depth habitat on carbonate $\delta^{18}O$ and $\delta^{13}C$. In general, $\delta^{18}O$ records are influenced by a combination of local temperature and salinity, and global ice volume variations (Chappell and Shackleton, 1986; Maslin et al., 1995; Rohling, 2000; Shackleton, 1974, 1987). If we assume constant ice volume for a snapshot in time, the foraminifera $\delta^{18}O$ signal mostly reflects the temperature of the water mass where it calcified (Mulitza et al., 2003; Schiebel and Hemleben, 2005; Schmidt and Mulitza, 2002). Therefore, $\delta^{18}O$ can be used to infer the depth habitat of different foraminifera species, with higher $\delta^{18}O$ indicating deeper and colder water masses (e.g., Mulitza et al. (1997), Rashid and Boyle (2007) and citations therein). Accordingly, lower $\delta^{18}O$ of *T. sacculifer* and *G. ruber* relative to *G. truncatulinoides*, *G. bulloides,* and *G. siphonifera* can be explained by their shallower depth habitats. Assuming constant $\delta^{18}O$ of seawater, we convert $\delta^{18}O$ of our most recent foraminiferal calcite data (2-3 Holocene samples) to temperature of calcification using an online tool ((Gaskell and Hull, 2022), version 1.2) and compare it with the modern temperature depth profile for a South Atlantic station (30.5°S, 34.5°W) close to our site (World Ocean Atlas, WOA18, (Locarnini et al., 2018)) (Fig. S6). Accordingly, the calcification depth for *T. sacculifer* and *G. ruber* is in ~19°C waters at ca. 100 m water depth. *Globigerinella siphonifera* calcify at ~16°C (i.e, ~200 m $\delta^{18}O$ depth) and *G. truncatulinoides* and *G. bulloides* have the lowest calcification temperature of ~11°C (i.e., ~ 400-500 m $\delta^{18}O$ depth). Previous studies in the South Atlantic subtropical gyre suggest a similar upper mixed layer depth habitat for *T. sacculifer* and *G. ruber* (Lessa et al., 2020). In contrast, both *G. siphonifera* Types I and II typically present maximum abundance between 50 m and 100 m water depth spanning the upper to lower deep chlorophyll maximum in the tropics and subtropical ocean (Rebotim et al., 2017; Schiebel and Hemleben, 2017; Schiebel et al., 2002), which is shallower than inferred from $\delta^{18}O$-derived calcification temperatures and a local temperature profile. The same type of discrepancy exists for *G. bulloides*, which typically dwells at surface to thermocline depths. This might suggest a non-local origin for these two species (see Section 4.4.3 on lateral transport).

Foraminiferal carbonate $\delta^{13}C$ is sensitive to the $\delta^{13}C$ of dissolved inorganic carbon (DIC) in ambient seawater (Zeebe and Wolf-Gladrow, 2001). Surface mixed layer DIC is generally enriched in ^{13}C due to photosynthesis, whereas subsurface water DIC $\delta^{13}C$ is lower due to bacterial respiration and remineralization of the low-$\delta^{13}C$ organic matter arriving from the euphotic zone (Kroopnick, 1985). In a stratified ocean, such as the South Atlantic subtropical gyre, shallow-dwelling foraminifera should thus incorporate a higher $\delta^{13}C$ in contrast to thermocline-dwellers with lower $\delta^{13}C$. At Site 516, the modern surface ocean $\delta^{13}C_{DIC}$ seems to be only marginally higher (~ 1.7 ‰) than the $\delta^{13}C_{DIC}$ in the upper thermocline (~ 1.4 ‰) (Fig.

S7). Calcite $\delta^{13}C$ of *T. sacculifer* and *G. truncatulinoides* at Site 516 generally follow the expected $\delta^{13}C_{DIC}$ depth relationship (Fig. S7). *G. ruber* and *G. siphonifera* $\delta^{13}C$ seem to be higher than *T. sacculifer* and are similar to the deeper dwelling *G. truncatulinoides*. *Globigerina bulloides* is a surface and thermocline-dweller and the only foraminifera species that exhibits a strongly depleted $\delta^{13}C$ signal with respect to other surface-dwelling foraminifera at Site 516. We suspect that this offset is due to other effects associated with symbiont respiration, seasonality (Section 4.4.2) or different environmental baseline for foraminifera originating from outside the South Atlantic gyre (Section 4.4.3).

Influence of seasonality on carbonate $\delta^{18}O$ and $\delta^{13}C$. In addition to depth habitat, the $\delta^{18}O$-derived temperature signal preserved in deep-sea sediments depends on seasonal changes in ocean temperatures and shell production and reflects an integrated signal across various seasons with a bias towards the season of highest production (Deuser and Ross, 1989; Tedesco et al., 2007; Thunell and Sautter, 1992). Based on foraminifera species counts in the North Atlantic, *T. sacculifer* records highest abundances in summer and fall. *Globigerinoides ruber* are associated with thermal maxima in the North Atlantic in summer. *Globigerinella siphonifera* appear to have a bimodal abundance distribution with peaks in spring and fall and *G. truncatulinoides* are an indicator of late winter/early spring conditions. The main production of *G. bulloides* occurs in spring (Salmon et al., 2015; Tolderlund and Bé, 1971). We expect similar seasonality of production at Site 516.

Biological and thermodynamic processes in the surface water and underlying water column, such as primary production, respiration, and air-sea gas exchange can potentially cause seasonal variability in DIC concentration and the $\delta^{13}C_{DIC}$ (Charles et al., 1993). However, shallow surface seawater data from the South Atlantic show only little variation between summer and winter. Throughout the year, surface $\delta^{13}C_{DIC}$ remains between 1.5‰ and 1.75 ‰ (Gruber et al., 1999). Therefore, we expect little or no effect of seasonality on interspecies-$\delta^{13}C$ in Site 516.

Results for nitrate $\delta^{15}N$ analyses. The vertical profiles of nitrate concentration ($[NO_3^-]$) from southern CLIMODE stations (<37.5 °N) show a distribution that is characteristic of the subtropical North Atlantic (Knapp et al., 2005). $[NO_3^-]$ decreases upward from an average of 24 µM near the base of the thermocline (800–1000 m) to 0–0.5 µM at the near-surface, with a depth zone of relatively constant $[NO_3^-]$ between 200 and 500 m that reflects 18° Water (Fig. S4). A strong latitudinal variation in $[NO_3^-]$ was observed in the typical upper thermocline depth zone (800–1000 m), increasing from 3–5 µM at the southernmost station to ~25 µM at northernmost station (38.6°N). Surface samples from the northernmost station have an average $[NO_3^-]$ of 3.2 µM which is comparable to $[NO_3^-]$ in the upper thermocline water at the BATS site.

The vertical structure of $\delta^{15}N$ in the southernmost CLIMODE stations is similar to that observed in the lower latitude Sargasso Sea (Fawcett et al., 2015; Knapp et al., 2005). The $\delta^{15}N$ starts to decrease from an average of ~5.3‰ at ~800 m depth and reaches its minimum of ~2.0‰ at ~200 m. Along the south to north CLIMODE transect, the upward decline in $\delta^{15}N$ becomes smaller, becoming absent in profiles from >38.0 °N. Every $\delta^{15}N$ profile shows a sharp rise toward the surface above ~200m depth, which is the effect of nitrate assimilation approaching completion in the euphotic zone (Fawcett et al., 2015).

The water masses from the Southern Ocean exhibit higher $[NO_3^-]$. The vertical profiles of $[NO_3^-]$ at the South Atlantic stations along the A13.5 transect reveal the highest $[NO_3^-]$ in the lower thermocline (~1200 m; characterized by Antarctic Intermediate Water, AAIW) and at the bottom depths (Antarctic Bottom Water, AABW). The North Atlantic Deep Water (NADW), occupying the depths between the AAIW and AABW, shows $[NO_3^-]$ around 25 µM. $[NO_3^-]$ decreases upward, from ~33 µM in the AAIW to near zero in stations north of 37.0°S, while the surface waters of the stations between 42°S and 41°S bear less than 7.6 µM of nitrate.

In terms of nitrate $\delta^{15}N$, the deep water in the South Atlantic stations shows values around 4.8‰ near the bottom, close to the mean nitrate $\delta^{15}N$ of NADW (Marconi et al., 2015). The nitrate $\delta^{15}N$ gradually increases upwards. From an average of ~5.2‰ at ~1500 m depth, $\delta^{15}N$ rises to ~6.6‰ at 200 m. As in the North Atlantic, nitrate $\delta^{15}N$ increases sharply toward the surface due to assimilation by phytoplankton (Fawcett et al., 2015).

Supplementary Tables:

Table S1. Slope and R^2 values for size-specific $\delta^{13}C$ measurements on different foraminifera species in Site 516.

	Glacial - 27 ka		Interglacial - 129 ka		combined	
	slope	**R^2**	**slope**	**R^2**	**slope**	**R^2**
T.sacculifer	0.0035	0.80	0.0071	0.93	0.0053	0.91
G.ruber albus	0.0050	0.95	0.0018	0.25	0.0034	0.76
G.ruber ruber	0.0035	0.95	0.0050	0.86	0.0043	0.91
G.truncatulinoides	0.0043	0.83	0.0038	0.46	0.0040	0.75
G.Siphoniphera	0.0013	0.36	0.0024	0.75	0.0018	0.60
G.bulloides	0.0028	1.00	0.0036	1.00	0.0032	1.00

Table S2. Core top FB-$\delta^{15}N$ compilation used for Figure 5 and 6.

core ID	short site ID	latitude	longitude	foraminifera species	reference
Barbuda-Antiqua	Barbuda-Antiqua	17.08	-61.03	*G. ruber albus, T. sacculifer, O. universa*	Ren et al., 2012
BATS	BATS	31.73	-64.08	*G. ruber albus, O. universa, G. menardii, N. dutertrei, G. hirsuta, G. inflata, G. truncatulinoides*	Smart et al., 2018
Cariaco Basin	Cariaco Basin	10.12	-64.12	*G. ruber albus, T. sacculifer, O. universa, G. menardii, G.dutertrei, G. siphonifera*	Ren et al., 2012
Cariaco Basin	Cariaco Basin	10.50	-64.70	*G. ruber albus, T. sacculifer, O. universa*	Schiebel et al., 2018
DSDP 516	DSDP 516	-30.28	-35.29	*G. ruber albus, G. ruber pink, T. sacculifer, G. siphonifera, G. truncatulinoides, G. bulloides*	this study
V25-75TW	Eq. Atlantic 1	8.58	-53.17	*G. ruber albus, T. sacculifer, O. universa*	Schiebel et al., 2018
Bill-22	Eq. Atlantic 2	7.00	-49.50	*G. ruber albus, T. sacculifer, O. universa*	Schiebel et al., 2018
RC13-184TW	Eq. Atlantic 3	3.87	-43.30	*G. ruber albus, T. sacculifer, O. universa*	Schiebel et al., 2018
V25-60TW	Eq. Atlantic 4	3.28	-34.83	*G. ruber albus, T. sacculifer, O. universa*	Schiebel et al., 2018
V25-59TW	Eq. Atlantic 5	1.37	-33.48	*G. ruber albus, T. sacculifer, O. universa*	Schiebel et al., 2018
V25-56TW	Eq. Atlantic 6	-3.55	-34.23	*G. ruber albus, T. sacculifer, O. universa*	Schiebel et al., 2018
V22-38TW	Eq. Atlantic 7	-9.55	-34.25	*G. ruber albus, T. sacculifer, O. universa*	Schiebel et al., 2018
RC13-189TW	Eq. Atlantic 8	1.87	-30.00	*G. ruber albus, T. sacculifer, O. universa*	Schiebel et al., 2018
V30-36TW	Eq. Atlantic 9	5.35	-27.32	*G. ruber albus, T. sacculifer, O. universa*	Schiebel et al., 2018
V30-40TW	Eq. Atlantic 10	-0.20	-23.15	*G. ruber albus, T. sacculifer, O. universa*	Schiebel et al., 2018
V30-41TW	Eq. Atlantic 11	0.22	-23.07	*G. ruber albus, T. sacculifer, O. universa*	Schiebel et al., 2018
V22-182TW	Eq. Atlantic 12	-0.55	-17.27	*G. ruber albus, T. sacculifer, O. universa*	Schiebel et al., 2018
39MC: 0-8	Eq. Pacific a	6.83	198.96	*G. ruber albus, T. sacculifer, G. tumida*	Costa et al., 2016
33MC: 0-8	Eq. Pacific b	5.20	199.57	*G. ruber albus, T. sacculifer, G. tumida*	Costa et al., 2016
26MC: 0-8	Eq. Pacific c	2.46	200.61	*G. ruber albus, T. sacculifer, G. tumida*	Costa et al., 2016
29MC: 0-8	Eq. Pacific d	2.97	200.80	*G. ruber albus, T. sacculifer, G. tumida*	Costa et al., 2016
21MC: 0-8	Eq. Pacific e	1.27	202.74	*G. ruber albus, T. sacculifer, G. tumida*	Costa et al., 2016
14MC: 0-8	Eq. Pacific f	-0.22	204.04	*G. ruber albus, T. sacculifer, G. tumida*	Costa et al., 2016
Great Bahama Banks	Great Bahama Banks	24.05	-79.03	*G. ruber albus, T. sacculifer, O. universa, G. menardii, G.dutertrei, G. siphonifera*	Ren et al., 2012
Hawaii	Hawaii	20.13	-157.05	*G. ruber albus, T. sacculifer*	Ren et al., 2012
Indonesia	Indonesia	-6.13	117.00	*G. ruber albus, T. sacculifer, O. universa, G. menardii, G.dutertrei, G. siphonifera*	Ren et al., 2012
New Zealand	New Zealand	-36.07	176.12	*G. ruber albus, O. universa, G. siphonifera*	Ren et al., 2012
ODP 1090	ODP 1090	-42.91	8.90	*O. universa, G. bulloides*	Martinez-Garcia 2014
ODP 662	ODP 662	-1.38	-11.78	*T. sacculifer, N. dutertrei*	Auderset et al., 2022
San Pedro Basin	San Pedro Basin	33.08	-118.08	*O. universa, N. dutertrei*	Ren et al., 2012
South China Sea	South China Sea	12.12	118.08	*G. ruber albus, T. sacculifer, O. universa, G. menardii, G.dutertrei, G. siphonifera*	Ren et al., 2012

Supplementary Figures:

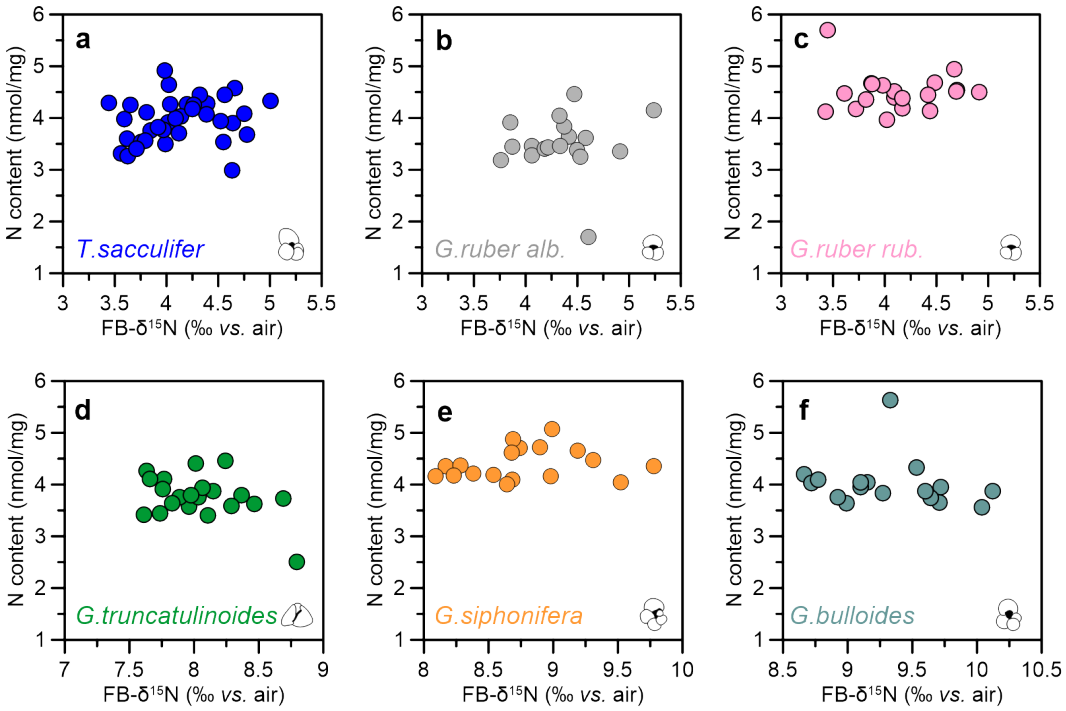

Figure S1. No correlation between N content and FB-δ^{15}N indicating no effect of diagenesis on FB-δ^{15}N signal.

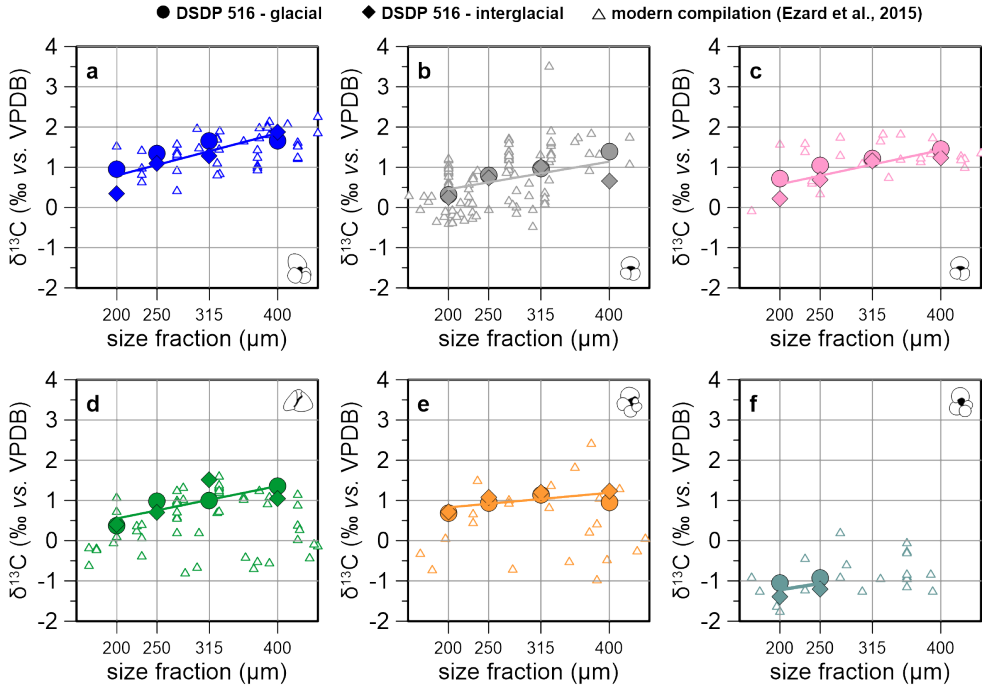

Figure S2. Size-specific $\delta^{13}C$ with linear fits. Carbon isotopes measured on calcite of **(a)** *T. sacculifer,* **(b)** *G. ruber albus* **(c)** *G.ruber ruber*, **(d)** *G. bulloides,* **(e)** *G. siphonifera,* and **(f)** *G. truncatulinoides* in DSDP 516 sediment samples from two time slices slices: 1-glacial, Last Glacial Maximum, 27 ka, circles and interglacial 2-interglacial, Marine Isotope Stage 5, 127 ka, diamonds. Data in comparison with size-specific carbon isotope compilation by Ezard et al. (2015) (triangles). Linear fit through average of size-specific $\delta^{13}C$ for both time slices in DSDP 516.

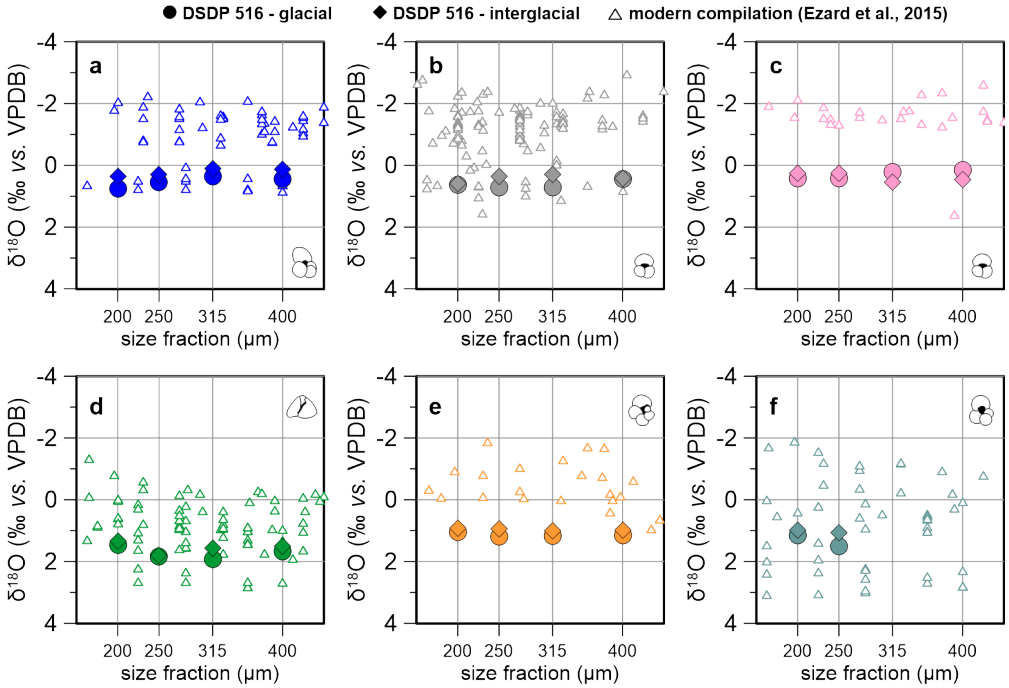

Figure S3. Size-specific $\delta^{18}O$. Oxygen isotopes measured on calcite of **(a)** *T. sacculifer,* **(b)** *G. ruber albus* **(c)** *G. ruber ruber*, **(d)** *G. bulloides,* **(e)** *G. siphonifera,* and **(f)** *G. truncatulinoides* in DSDP 516 sediment samples from two time slices: 1-glacial, Last Glacial Maximum, 27 ka, circles and interglacial 2-interglacial, Marine Isotope Stage 5, 127 ka, diamonds. Data in comparison with size-specific oxygen isotope compilation by Ezard et al. (2015) (triangles).

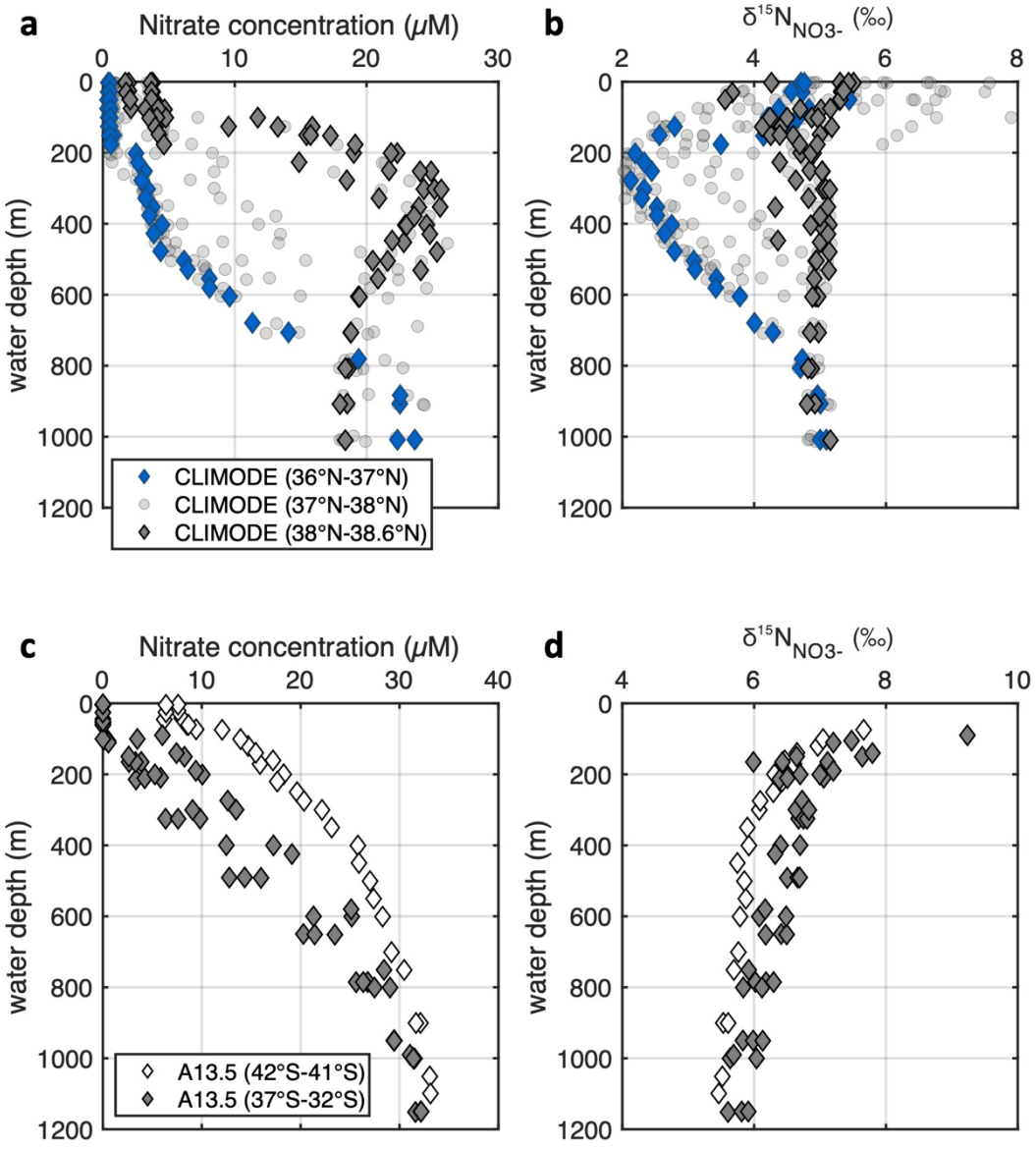

Figure S4. Nitrate concentration and nitrate $\delta^{15}N$ depth profiles. (a) Nitrate concentration in μM and (b) and nitrate $\delta^{15}N$ (‰ *vs.* air) in CLIMODE stations in the North Atlantic, divided into three groups (36-37ºN, 37-38 ºN and 38-38.6ºN). (c) Nitrate concentration in μM and (d) and nitrate $\delta^{15}N$ (‰ *vs.* air) in A13.5 stations in the South Atlantic, divided into two groups (42-41ºS and 37-32ºS).

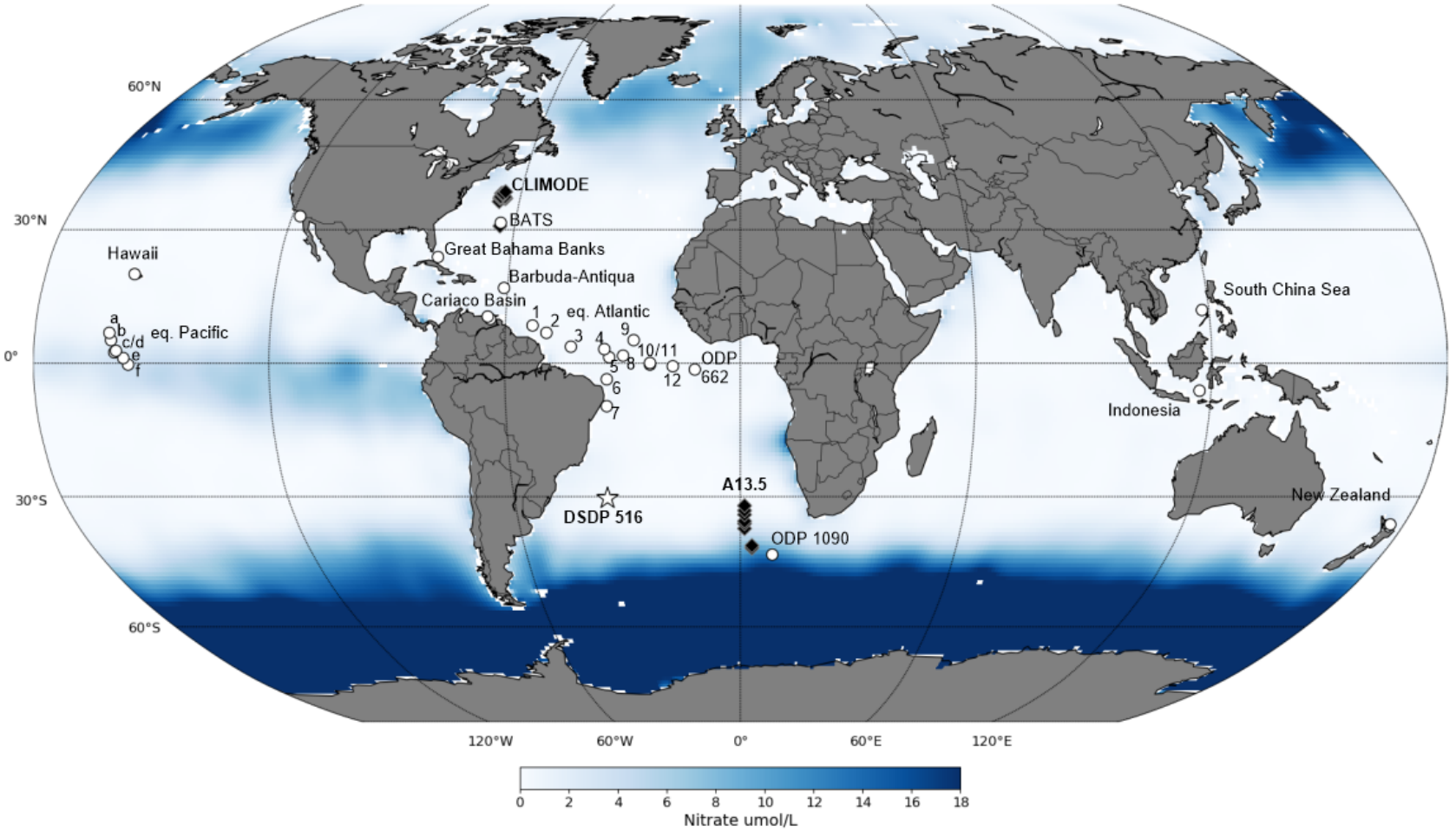

Figure S5. Global core top compilation of published FB-δ^{15}N data used in Figure 5 and 6. Core locations plotted on mean annual surface nitrate map. Data from (Garcia et al., 2013). Map generated with Python-based Matplotlib Basemap toolkit (Whitaker and Matplotlib-Team, 2024). Detailed information about core sites, coordinates, analysed species and references can be found in Table S2.

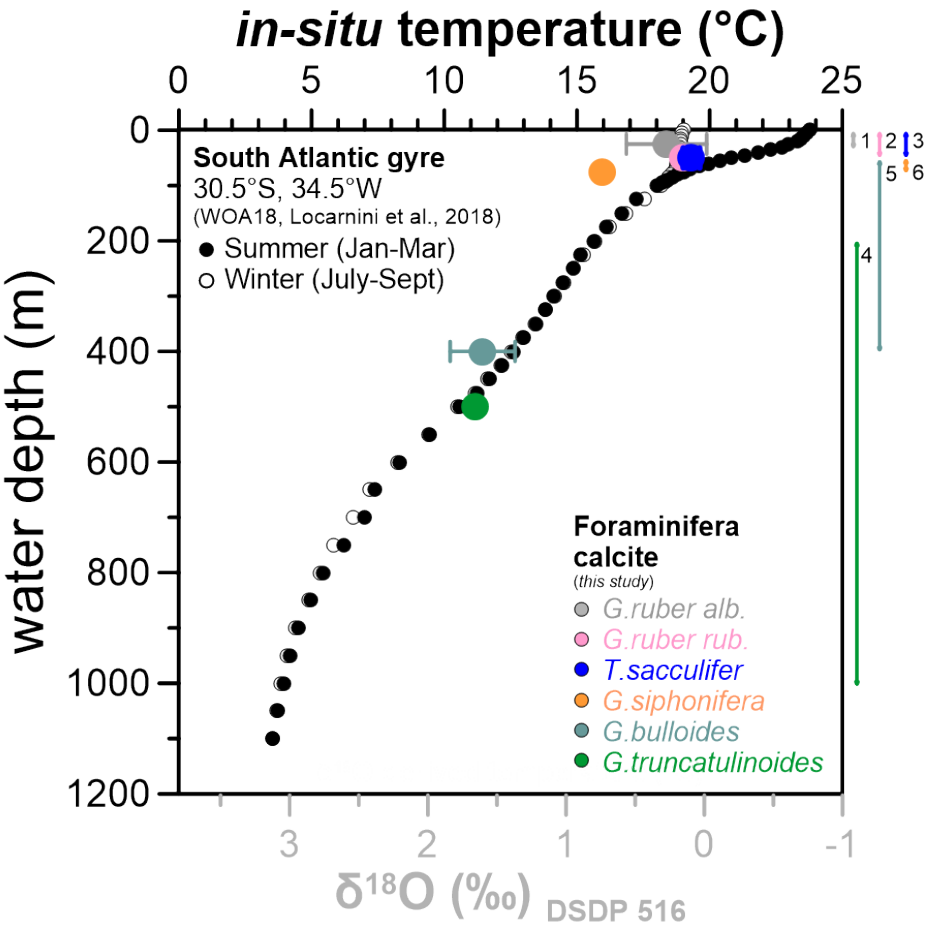

Fig. S6. Temperature depth profile in comparison with oxygen isotopes measured in foraminiferal calcite in DSDP Site 516. Average of $\delta^{18}O$ in various foraminifera species in Site 516 (read values from grey x-axis) and $\delta^{18}O$-derived temperatures using an online tool (Gaskell and Hull (2022), version 1.2) overlying temperature depth profile approximate depth habitat for each foraminifera species. *In-situ* temperatures in South Atlantic gyre (for winter months (open circles) and summer months (filled circles) (World Ocean Atlas, WOA18, (Locarnini et al., 2018)) (read values from black x-axis). Colored bars at the right indicate proposed depth habitats for analysed foraminifera from the literature: [1]*G. ruber albus* in surface mixed layer (<25m), [2]*G. ruber ruber* in surface mixed layer (<50m), [3]*T. sacculifer* in surface mixed layer (<50m, [4]*G. truncatulinoides* in thermocline/sub-thermocline, [5]*G. bulloides* in surface mixed layer/thermocline (<400 m) and [6]*G. siphonifera* in surface mixed layer (50-75m) (Bé et al., 1977; Hemleben et al., 1989).

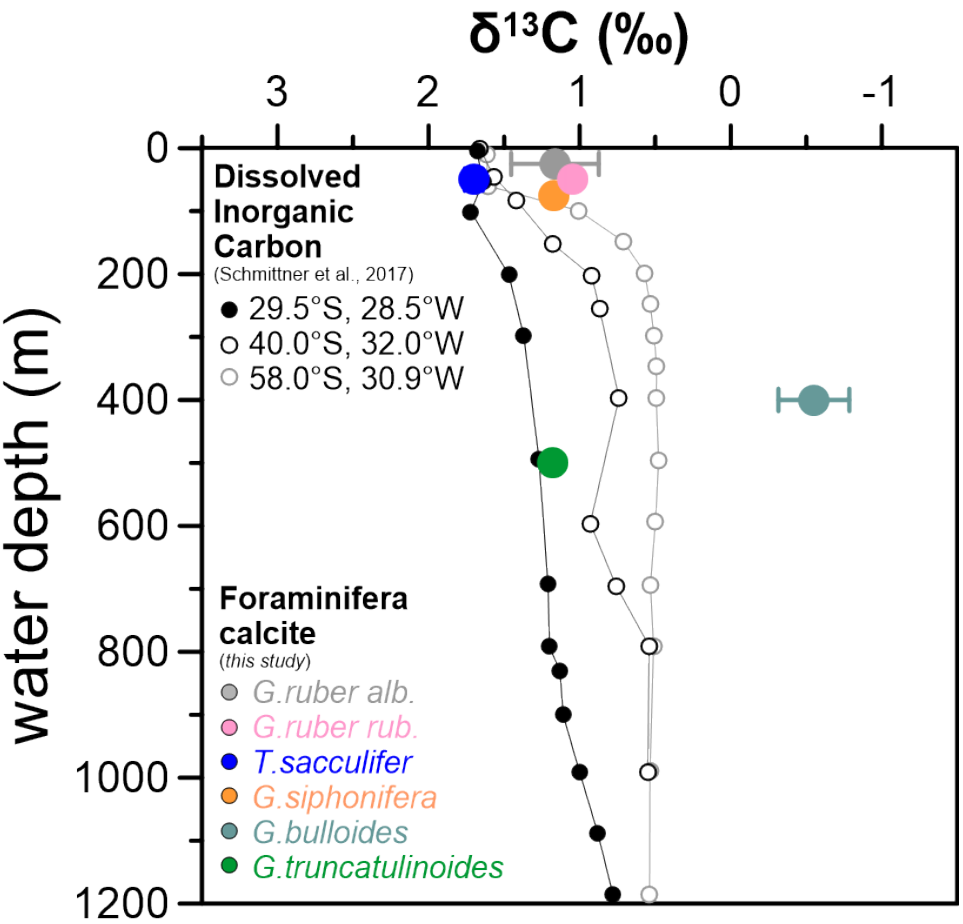

Fig. S7. Dissolved Inorganic Carbon (DIC) carbon isotope depth profile in comparison with carbon isotopes measured on foraminiferal calcite in DSDP Site 516. Average of Holocene $\delta^{13}C$ measured on species-specific foraminiferal calcite in Site 516. $\delta^{13}C_{DIC}$ from South Atlantic stations close to Site 516 (29.5ºS, 28.5ºW, black) and locations further south (40.0ºS, 32.0ºW, open black circle and 58.0ºS, 30.9ºW, open grey circle) (Schmittner et al., 2017).

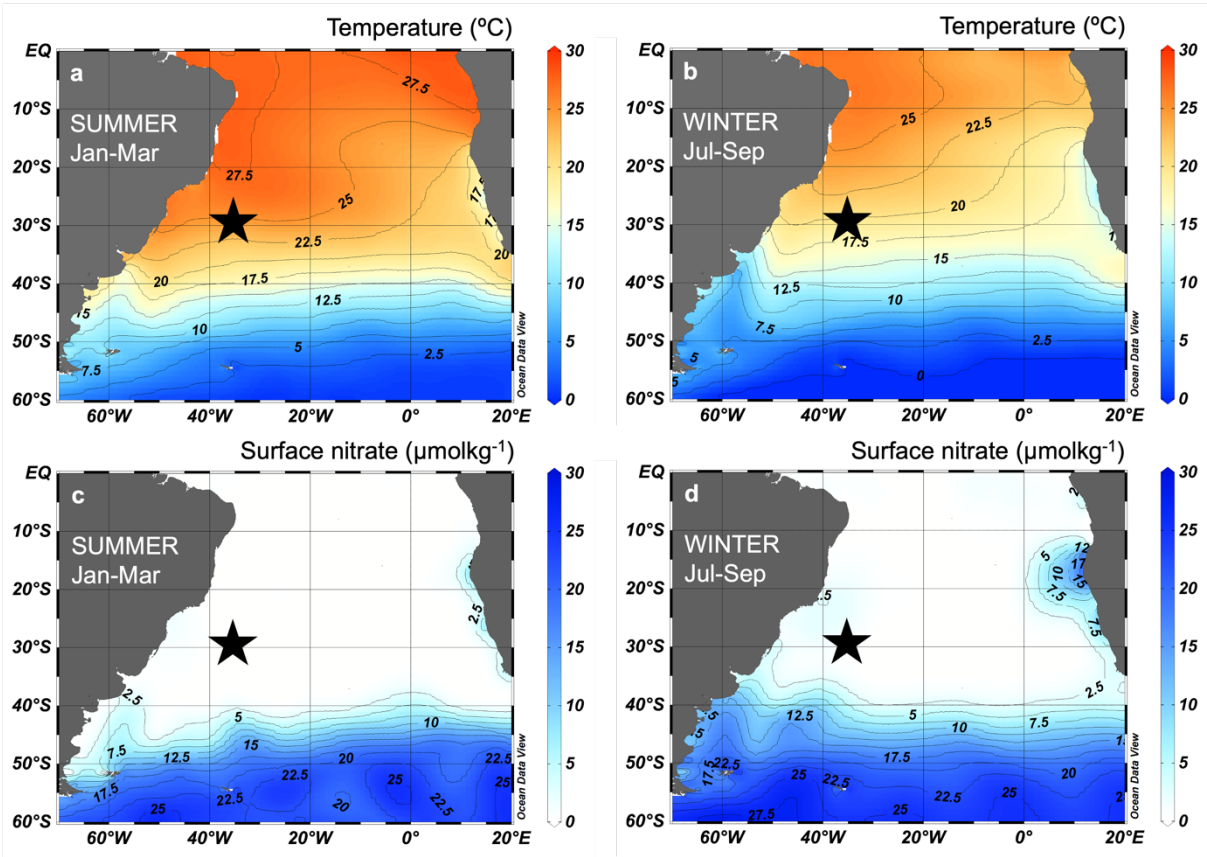

Figure S8. **Summer (January to March) and winter (July to September) surface maps for the South Atlantic. (a,b)** sea surface temperature (in ºC), **(c,d)** surface nitrate (in µmol/kg). Black star indicates location for studied core site DSDP 516. Map generated with Ocean Data View (Schlitzer, 2015) and data set from World Ocean Atlas 18 (Garcia et al., 2013; Locarnini et al., 2018).

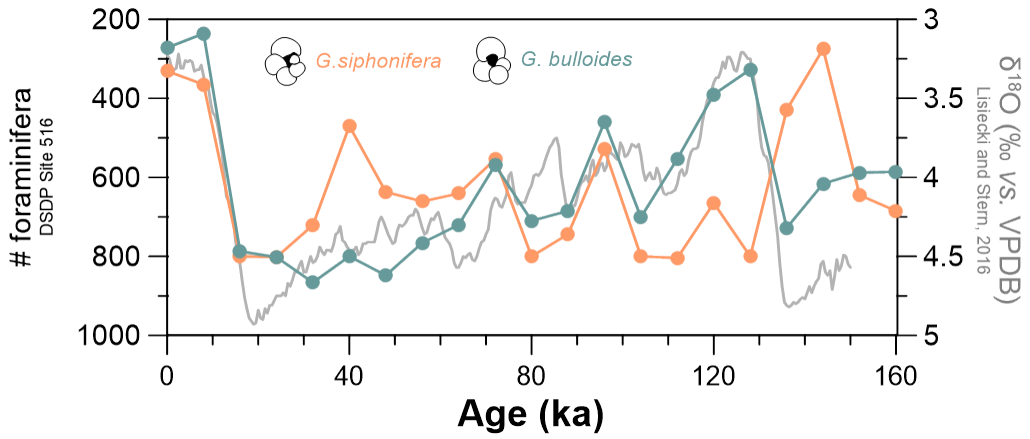

Figure S9. Counted foraminifera specimen per 5cc of sediment in DSDP 516. Orange dots indicate counts for *G. siphonifera*, turquoise dots indicate counts for *G. bulloides*. Note that we stopped counting if number of specimens reached 800 for *G. siphonifera.*

References for Supplementary Material:

Bé, A. W., Hemleben, C., Anderson, O. R., Spindler, M., Hacunda, J., and Tuntivate-Choy, S., 1977, Laboratory and field observations of living planktonic foraminifera: Micropaleontology, p. 155-179.

Fawcett, S. E., Ward, B. B., Lomas, M. W., and Sigman, D. M., 2015, Vertical decoupling of nitrate assimilation and nitrification in the Sargasso Sea: Deep Sea Research Part I: Oceanographic Research Papers, v. 103, p. 64-72.

Garcia, H. E., Locarnini, R. A., Boyer, T. P., Antonov, J. I., Baranova, O. K., Zweng, M. M., Reagan, J. R., Johnson, D. R., Mishonov, A. V., and Levitus, S., 2013, World ocean atlas 2013. Volume 4, Dissolved inorganic nutrients (phosphate, nitrate, silicate).

Gaskell, D. E., and Hull, P. M., 2022, A new online tool for δ18O-temperature conversions: Climate of the Past Discussions, v. 2022, p. 1-11.

Hemleben, C., Spindler, M., and Anderson, O. R., 1989, Modern planktonic foraminifera, Springer Science & Business Media.

Knapp, A. N., Sigman, D. M., and Lipschultz, F., 2005, N isotopic composition of dissolved organic nitrogen and nitrate at the Bermuda Atlantic Time-series Study site: Global Biogeochemical Cycles, v. 19, no. 1.

Locarnini, M., Mishonov, A., Baranova, O., Boyer, T., Zweng, M., Garcia, H., Seidov, D., Weathers, K., Paver, C., and Smolyar, I., 2018, World ocean atlas 2018, volume 1: Temperature.

Schlitzer, R., 2015, Data analysis and visualization with Ocean Data View: CMOS Bulletin SCMO, v. 43, no. 1, p. 9-13.

Schmittner, A., Bostock, H. C., Cartapanis, O., Curry, W. B., Filipsson, H. L., Galbraith, E. D., Gottschalk, J., Herguera, J. C., Hoogakker, B., and Jaccard, S. L., 2017, Calibration of the carbon isotope composition (δ13C) of benthic foraminifera: Paleoceanography, v. 32, no. 6, p. 512-530.

Whitaker, J., and Matplotlib-team, T., 2024, Basemap 1.4.1 documentation.